Title: Mechanisms of synaptic zinc plasticity at mouse dorsal cochlear nucleus glutamatergic synapses

Authors: Nathan W. Vogler[1] and Thanos Tzounopoulos[*1]

[1]Department of Otolaryngology and Pittsburgh Hearing Research Center, University of Pittsburgh, Pittsburgh, PA 15261

* To whom correspondence may be addressed. Email: thanos@pitt.edu

In many excitatory synapses, synaptic zinc is co-released with glutamate to modulate neurotransmission. Synaptic zinc modulates the responsiveness of auditory cortex to sound, and synaptic zinc levels and signaling are modulated by sensory experience, termed zinc plasticity. The mechanisms underlying zinc plasticity remain unknown. We discovered that high- and low-frequency electrical stimulation of dorsal cochlear nucleus synapses reduces and increases synaptic zinc signaling, respectively. This bidirectional zinc plasticity is evidenced by changes in zinc inhibition of AMPA and NMDA receptor activity. Increases and decreases in zinc signaling require activation of Group 1 metabotropic glutamate receptors (mGluRs). Activation of Group 1 mGluRs with a higher agonist concentration increases presynaptic zinc levels and postsynaptic zinc signaling, whereas activation with a lower concentration reduces zinc levels and signaling. Sound-induced zinc plasticity also requires Group 1 mGluRs. Our results reveal the mechanisms underlying synaptic zinc plasticity, elicited by either synaptic activity or sound experience.

Introduction

In many brain areas, including the neocortex, limbic structures, and the auditory brainstem, glutamatergic vesicles are loaded with zinc (Danscher & Stoltenberg, 2005; Frederickson et al., 2005). This pool of mobile, synaptic zinc is co-released with glutamate and is a major modulator of glutamatergic neurotransmission. Namely, synaptic zinc inhibits synaptic and extrasynaptic NMDA receptor (NMDAR) excitatory postsynaptic currents (EPSCs), and modulates AMPA receptor (AMPAR) EPSCs (Kalappa et al., 2015; 2017; Anderson et al., 2015; Vogt et al., 2000; Vergnano et al., 2014). Synaptic zinc inhibits AMPAR EPSCs at lower frequencies of synaptic activity, but enhances steady state AMPAR EPSCs during higher frequencies of activity by recruiting endocannabinoid signaling, reducing probability of release and enhancing synaptic facilitation (Kalappa et al., 2015; 2017; Perez-Rosello et al., 2013). In awake mice, synaptic zinc enhances the responsiveness (gain) of sound-evoked responses in auditory cortical principal neurons but reduces the gain of cortical interneurons (Anderson et al., 2017). Activity-dependent changes in gain are crucial for sensory processing, for they allow sensory systems to adapt to changing sensory environments and facilitate central recovery of sensory processing in response to peripheral damage (Atallah et al., 2012; Ohshiro et al., 2011; Dean et al., 2005; Watkins & Barbour, 2008; Rabinowitz et al., 2011; Natan et al., 2017; Chambers et al., 2016; Resnik et al., 2017).

Consistent with the role of synaptic zinc in gain modulation of sound-evoked responses, sensory experience bidirectionally modulates the levels of vesicular zinc and synaptic zinc signaling in several sensory brain areas (Nakashima & Dyck, 2009; Li et al., 2017; Kalappa et al., 2015; McAllister & Dyck, 2017). In the somatosensory cortex, whisker plucking increases zinc levels, whereas whisker stimulation reduces zinc levels (Brown & Dyck 2002; 2005). In the primary visual cortex, monocular deprivation increases vesicular zinc levels (Dyck et al., 2003). In the retina, optic nerve damage increases zinc levels, which in turn inhibit optic nerve regeneration and

promote cell death (Li et al., 2017). In the dorsal cochlear nucleus (DCN), an auditory brainstem nucleus, exposure to loud sound reduces vesicular zinc levels and synaptic zinc signaling (Kalappa et al., 2015). Yet, the cellular and molecular mechanisms underlying the experience-dependent plasticity of synaptic zinc levels remain unknown. Elucidating these mechanisms is crucial for understanding how the brain adapts during normal sensory processing, and why it fails to properly adjust in sensory disorders associated with pathological central adaptation, such as in tinnitus (Auerbach et al., 2014).

To determine the mechanisms of zinc plasticity, we used electrophysiology and fluorescent imaging in the DCN, which contains parallel fibers (PFs) with high levels of synaptic zinc that are modulated by sound experience (Frederickson et al., 1988; Rubio & Juiz, 1998; Kalappa et al., 2015). We investigated these mechanisms *in vitro*, in response to electrical synaptic activation in brain slices, as well as *in vivo*, in response to loud sound exposure. Our results demonstrate bidirectional activity-dependent zinc plasticity, and reveal a novel mechanism of plasticity in central synapses that involves mGluR activation.

Results

Bidirectional activity-dependent zinc plasticity requires Group 1 mGluRs

To investigate the mechanisms underlying zinc plasticity, we first determined whether we could induce zinc plasticity in DCN PF synapses in mouse brain slices. In these synapses, application of the fast, high-affinity extracellular zinc chelator ZX1 potentiates AMPAR and NMDAR EPSCs via postsynaptic mechanisms (Anderson et al., 2015; Kalappa et al., 2015; 2017). Moreover, this potentiation is dependent on ZnT3, the transporter that loads zinc into synaptic vesicles (Palmiter et al., 1996; Cole et al., 1999), indicating that synaptic zinc inhibits AMPAR and NMDAR EPSCs. We therefore used the ZX1 potentiation of AMPAR and NMDAR EPSCs, as well as imaging of presynaptic zinc levels, as assays for monitoring zinc plasticity in the DCN.

Consistent with previous studies, we found that ZX1 potentiated postsynaptic PF AMPAR EPSCs in DCN cartwheel cells (CWCs), a class of inhibitory interneurons (Fig. 1 A-B) (Kalappa et al., 2015; 2017). To develop an *in vitro* model of zinc plasticity to study underlying mechanisms, we tested whether we can induce zinc plasticity by using patterns of synaptic activation that induce plasticity of glutamatergic signaling, such long-term potentiation and depression (LTP/LTD) in the DCN PF synapses (Tzounopoulos et al., 2004; 2007; Fujino & Oertel, 2003). We started by examining the effect of ZX1 on AMPAR EPSCs following high-frequency stimulation of PFs (HFS, 3 x 100 Hz for 1 sec, 10 sec inter-stimulus interval), which induces glutamatergic LTP (Fujino & Oertel, 2003). After applying HFS and obtaining a new stable baseline, we renormalized AMPAR EPSC amplitude to the new baseline, to quantify the amount ZX1 potentiation after HFS (Fig. 1 C). After HFS, ZX1 application did not potentiate AMPAR EPSCs (Fig. 1 C-D). The loss of ZX1 potentiation indicates a loss of zinc-mediated inhibition of AMPARs, suggesting that HFS caused a reduction in synaptic zinc signaling, thereby inducing zinc plasticity.

After establishing that HFS reduced zinc signaling, we then used this stimulation paradigm as a tool for studying the underlying mechanisms. NMDARs mediate the induction of LTP and LTD in the DCN and most central synapses (Malenka & Nicoll, 1993; Tzounopoulos et al., 2004; 2007; Fujino & Oertel, 2003). To test the role of NMDARs in the induction of zinc plasticity by HFS, we blocked NMDARs with APV (NMDAR antagonist, 50 μM; Fig. 2 A). As evidenced by the lack of ZX1 potentiation of AMPAR EPSCs after HFS, APV did not affect HFS-induced reductions in zinc signaling (Fig. 2 A, C), suggesting that NMDARs are not required for the induction of zinc plasticity.

Parallel fiber synapses in the DCN also exhibit glutamatergic plasticity that involves metabotropic glutamate receptor (mGluR) signaling (Fujino & Oertel, 2003). Furthermore, Group 1 mGluRs are

expressed in CWCs and in the DCN molecular layer, which contains PF terminals (Wright et al., 1996; Bilak & Morest, 1998). We therefore tested whether Group 1 mGluR signaling is necessary for the induction of zinc plasticity. To test this hypothesis, we repeated the experiment shown in 2A, but now we blocked Group 1 mGluRs with MPEP (4 μM, mGluR5-selective antagonist) and LY367385 (100 μM, mGluR1-selective antagonist) (Fig. 2 B). Under these conditions, HFS did not affect ZX1 potentiation compared to control, no HFS, conditions (Fig. 2 B-C), suggesting that Group 1 mGluR activation is necessary for the induction of zinc plasticity by HFS.

Glutamatergic plasticity is bidirectional: synapses undergo LTP or LTD in response to high- or low-frequency stimulation, respectively (Malenka & Nicoll, 1993; Mulkey & Malenka, 1992; Fujino & Oertel 2003). To determine whether zinc plasticity is bidirectional, we tested whether low-frequency stimulation (LFS) increases zinc signaling (Fig. 3 A). Because the induction of zinc plasticity depends on mGluR activation, we used conditions that favor mGluR activation such as LFS (5 Hz, 3 min), blockade of NMDARs with APV, and high extracellular concentrations of divalent ions (4 mM Ca^{2+} and Mg^{2+}; Oliet et al., 1997). Compared to control (no LFS), LFS increased the amount of ZX1 potentiation (Fig. 3 A, C). Note that control ZX1 potentiation in these conditions (Fig. 3 C) was slightly less, albeit not significantly different (p=0.11, unpaired t test), than previous control experiments performed in ACSF with 2.4/1.3 mM of extracellular Ca^{2+}/Mg^{2+} (Fig. 1 D). This is likely due to reduced neuronal excitability (Oliet et al., 1997; Kalappa et al., 2015). Together, these results suggest that LFS increased synaptic zinc signaling, thus demonstrating that activity-dependent plasticity of zinc signaling is bidirectional: HFS reduces zinc signaling, whereas LFS increases zinc signaling.

We next tested whether Group 1 mGluR activation is necessary for the increased zinc signaling by LFS. Whereas LFS alone increased ZX1 potentiation compared to control, LFS in the presence

of MPEP and LY367385 did not increase ZX1 potentiation (Fig. 3 B-C). This indicates that Group 1 mGluR activation is necessary for the induction of zinc plasticity by LFS. Together, these results reveal that activation of Group 1 mGluR signaling is necessary for the induction of bidirectional zinc plasticity by HFS or LFS.

Group 1 mGluR activation is sufficient to induce bidirectional zinc plasticity

Is activation of Group 1 mGluRs sufficient to induce zinc plasticity? Because Group 1 mGluRs are required for both increases and decreases in zinc signaling by different stimulation paradigms, we hypothesized that the direction of plasticity depends on differential activation of mGluRs during the induction protocols. To test this, we applied high or low concentrations of DHPG (Group 1 mGluR agonist, 50 μM or 5 μM). Consistent with previous studies, application of 50 μM DHPG caused LTD (Fig. 4 A; Huber et al., 2001; Wisniewski & Car, 2002; Snyder et al. 2001). After applying 50 μM DHPG, obtaining a new stable baseline, and then applying ZX1, we observed that the ZX1 potentiation of EPSCs was significantly increased compared to control (Fig. 4 A, C-D). This result indicates that a high concentration of DHPG increases zinc signaling: Group 1 mGluR activation is sufficient to induce zinc plasticity.

Because increases and decreases in zinc signaling induced by L/HFS depend on Group 1 mGluR activation (Fig. 2 and 3), we next tested whether application of a lower concentration of DHPG reduces zinc signaling. After applying 5 μM DHPG and obtaining a new stable baseline, ZX1 did not potentiate EPSCs (Fig. 4 B-D). This result indicates that activation of Group 1 mGluRs with a lower concentration of DHPG reduces zinc signaling. Together, these results demonstrate that Group 1 mGluR activation is sufficient to induce bidirectional zinc plasticity. Furthermore, the direction of zinc plasticity depends on the concentration of DHPG: 50 μM DHPG increases zinc signaling, whereas 5 μM DHPG reduces zinc signaling. These results are consistent with the

notion that bidirectional zinc plasticity depends on differential activation of Group 1 mGluRs by either L/HFS or high/low concentrations of DHPG.

Group 1 mGluR activation bidirectionally modulates presynaptic zinc levels

We used activity-dependent changes in the amount of ZX1 potentiation of AMPAR EPSCs for assessing changes in zinc signaling. However, ZX1 potentiation is determined by the postsynaptic zinc-mediated inhibition of AMPAR EPSCs, as well as the amount of presynaptic zinc release (Kalappa et al., 2015). Because previous studies have demonstrated activity-dependent modulation of presynaptic zinc levels (Nakashima & Dyck, 2009; Kalappa et al., 2015), we hypothesized that the plasticity of zinc signaling is due, at least in part, to the modulation of presynaptic zinc levels. To quantify potential changes in presynaptic zinc levels, we used DA-ZP1 (0.5 μM), a fluorescent intracellular zinc sensor capable of tracking presynaptic zinc levels in PF terminals (Kalappa et al., 2015; Zastrow et al., 2016). To induce zinc plasticity, we applied DHPG, which, unlike synaptic stimulation, induces zinc plasticity in all terminals in the slice. We imaged DA-ZP1 fluorescence (Fig. 5 A) in control slices and in slices treated with DHPG (50 μM or 5 μM). Compared to the non-treated control slices, incubation of slices with 50 μM DHPG increased DA-ZP1 fluorescence in the DCN molecular layer, indicating increased presynaptic zinc levels in PF terminals (Fig. 5 B). In contrast, incubation of slices with 5 μM DHPG reduced DA-ZP1 fluorescence, indicating reduced zinc levels (Fig. 5 B). These results demonstrate that application of different concentrations of DHPG causes bidirectional modulation of presynaptic zinc levels. Furthermore, these results are consistent with our electrophysiological experiments: 50 μM DHPG increases zinc levels and ZX1 potentiation of EPSCs, whereas 5 μM DHPG reduces zinc levels and ZX1 potentiation of EPSCs. Although our results do not rule out potential postsynaptic mechanisms of zinc plasticity, our results demonstrate that zinc plasticity involves modulation of presynaptic zinc levels.

Zinc plasticity does not depend on AMPAR plasticity, and it affects zinc-mediated inhibition of NMDARs

Pharmacological or electrophysiological induction of zinc plasticity is consistent with modulation of presynaptic zinc levels, but postsynaptic modifications are also possible. Because PFs exhibit postsynaptic AMPAR LTP (Fujino & Oertel, 2003; Tzounopoulos et al., 2007; Zhao & Tzounopoulos, 2011), we therefore sought to determine whether ZX1 potentiation is correlated with the amount of AMPAR LTP. To test for this, we plotted the ZX1 potentiation versus the changes in AMPAR EPSC amplitude after HFS (Fig. 6 A). We found no correlation between AMPAR plasticity and ZX1 potentiation (Fig. 6 A). This result suggests that modulation of zinc signaling does not depend on the amount of AMPAR potentiation, and supports the notion that modification of postsynaptic AMPARs during LTP are likely not involved in zinc plasticity.

Our DA-ZP1 imaging results suggest that zinc plasticity involves modulation of presynaptic zinc signaling. Therefore, the induction of zinc plasticity should also affect postsynaptic NMDAR EPSCs, which are inhibited by zinc via direct high-affinity receptor binding (Paoletti et al., 1997; Vergnano et al., 2014). To test this hypothesis, we quantified the ZX1 potentiation of NMDAR EPSCs after inducing zinc plasticity with HFS. To monitor NMDAR EPSCs, we used a short train of presynaptic stimulation (5 pulses at 20 Hz) to activate extrasynaptic NMDARs, for NMDAR EPSCs recorded in somata of CWCs are mostly mediated by extrasynaptic NMDARs activated by glutamate spillover during this short train (Anderson et al., 2015). To avoid keeping CWCs at +40 mV for too long while recording NMDAR EPSCs, and to maintain the same induction protocol used in our previous experiments, we initially recorded AMPAR EPSCs at -70 mV, then applied HFS. Subsequently, we blocked AMPARs with DNQX (20 μM, AMPA/kainate receptor antagonist) and recorded at +40 mV to obtain a stable baseline of NMDAR EPSCs before applying ZX1 (Fig. 6 B). Consistent with our results on AMPAR EPSCs, after HFS, ZX1 no longer potentiated NMDAR EPSCs (Fig. 6 B, D), whereas ZX1 enhanced NMDARs EPSCs in interleaved control

experiments where HFS was not applied, also consistent with previous results from DCN CWCs (Anderson et al., 2015). These results demonstrate that HFS-induced zinc plasticity reduces zinc-mediated inhibition of NMDARs. To determine whether this modulation shares the same mechanism with the zinc plasticity evidenced by changes in the ZX1 potentiation of AMPAR EPSCs, we tested whether Group 1 mGluR signaling is required. Indeed, application of MPEP and LY367385 blocked the observed zinc plasticity (Fig. 6 C-D), demonstrating that Group 1 mGluR signaling is required for HFS-induced plasticity of NMDAR zinc inhibition.

Finally, to control for potential non-specific effects of ZX1 on presynaptic zinc levels, perhaps through redistribution of zinc levels in different cellular compartments, we tested the effect of ZX1 on DA-ZP1 fluorescence. Indeed, application of ZX1 10 min prior and during DA-ZP1 application did not affect the fluorescence levels in the molecular layer of the DCN (Fig. 6 E). This result indicates that ZX1 does not affect presynaptic zinc levels, and is consistent with the notion that changes in the ZX1 potentiation of EPSCs after L/HFS detect activity-dependent changes in presynaptic zinc levels and signaling.

Together, our results indicate that pharmacological or synaptic activation of Group 1 mGluRs causes bidirectional synaptic zinc plasticity. Synaptic zinc plasticity modulates zinc inhibition of NMDARs and AMPARs, suggesting that it is, at least in part, expressed by activity-dependent changes of presynaptic zinc levels, regardless of the postsynaptic effector of zinc.

Sound-dependent zinc plasticity requires Group 1 mGluRs *in vivo*

Our experiments described here, using *in vitro* brain slice electrophysiology and fluorescent imaging in the DCN, point toward a mechanism of bidirectional plasticity of presynaptic zinc levels mediated by Group 1 mGluR signaling. We therefore hypothesized that mGluR activation may also be necessary for the sound-dependent zinc plasticity observed in the DCN (Kalappa et al.,

231 2015). To test this hypothesis, we examined DA-ZP1 fluorescence, and ZX1 potentiation of
232 EPSCs, in DCN slices from mice exposed to loud sound (116 dB, 4 hours). Consistent with
233 previous studies (Kalappa et al., 2015), slices from noise-exposed (N.E.) mice exhibited reduced
234 DA-ZP1 fluorescence in the molecular layer, indicating reduced presynaptic zinc levels, compared
235 to slices from control, sham-exposed, mice (Fig. 7 A). To test whether Group 1 mGluRs are
236 necessary for the sound-induced plasticity of zinc levels, we administered a systemic, blood brain
237 barrier-permeable Group 1 mGluR antagonist (AIDA, i.p., 2 mg/kg) twice: 30 min before and 1.5
238 hours after beginning the noise exposure. Slices from N.E. mice treated with AIDA did not show
239 changes in DA-ZP1 fluorescence (Fig. 7 A), suggesting that inhibition of Group 1 mGluR activity
240 blocked the sound-induced reduction of presynaptic zinc levels. Moreover, because N.E. mice
241 given vehicle (saline) treatment showed normal reductions in zinc levels, and AIDA treatment in
242 sham-exposed mice caused no change in zinc levels (Fig. 7 A), these results suggest that Group
243 1 mGluR activation is necessary for sound-induced changes of presynaptic zinc levels, but does
244 not affect baseline zinc levels.
245
246 To test whether Group 1 mGluRs are required for sound-induced reductions in synaptic zinc
247 signaling, we quantified the ZX1 potentiation of AMPAR EPSCs in DCN slices from N.E. mice and
248 N.E., AIDA-treated mice (Fig. 7 B-C). Consistent with previous studies (Kalappa et al., 2015), and
249 the reduction of presynaptic zinc levels after noise exposure (Fig 7 A), ZX1 potentiation was not
250 observed in slices from N.E. mice (Fig. 7 B-C). However, in slices from N.E., AIDA-treated mice,
251 ZX1 potentiation was observed (Fig. 7 B-C). Together, these results indicate that Group 1 mGluRs
252 are required for sound-induced plasticity of presynaptic zinc levels and zinc signaling.
253 Furthermore, although AIDA treatment blocked zinc plasticity in DCN PF synapses (Fig. 7 A-C),
254 it did not affect assays that are sensitive to presynaptic glutamate release probability, such as
255 paired-pulse ratio (PPR) and coefficient of variation (CV) analysis (Fig. 7 D). This indicates that
256 mGluR-dependent zinc plasticity specifically modulates presynaptic zinc levels and zinc signaling,

257 without affecting presynaptic glutamate signaling in PFs. Furthermore, AIDA treatment did not
258 affect sound-induced hearing loss in N.E. mice, quantified using Auditory Brainstem Responses
259 (ABRs) (Fig. 7 E). ABRs reflect the synchronous activity, arising from the auditory nerve (Wave
260 I), of auditory brainstem nuclei to the inferior colliculus (Waves II-V) in response to sound stimuli.
261 Elevated ABR thresholds indicate increased hearing thresholds. In N.E. mice, because no ABRs
262 were detected when recording from the exposed (ipsilateral) ear, we recorded ABRs from the
263 non-exposed (contralateral) ear (Fig. 7 E). Moreover, similar ABR thresholds may be
264 accompanied by differences in the suprathreshold response of Wave I, which could reflect
265 differential degeneration of the auditory nerve (Kujawa & Liberman, 2009). AIDA treatment did
266 not affect noise-induced changes in either ABR thresholds or Wave I amplitude (Fig. 7 F), thus
267 indicating that the effect of AIDA on blocking zinc plasticity is not due to differential noise-induced
268 hearing loss after AIDA treatment. Together, these results demonstrate that Group 1 mGluR
269 signaling is required for sound-dependent zinc plasticity *in vivo*.
270
271 **Discussion**
272 Our results show that zinc plasticity is an experience- and mGluR-dependent process that
273 bidirectionally modulates synaptic zinc levels and signaling in the DCN. Is this a general
274 mechanism that applies to all synaptic zinc-containing brain areas? Synaptic zinc is present
275 throughout the neocortex and other brain structures, such as the amygdala and the hippocampus
276 (McAllister & Dyck, 2017). Moreover, synaptic zinc is modulated by sensory activity throughout
277 the sensory cortex (McAllister & Dyck, 2017), shapes the gain of central sensory responses
278 (Anderson et al., 2017), and when upregulated by optic nerve injury, it inhibits retinal ganglion cell
279 survival and axon regeneration (Li et al., 2017). It is therefore likely, although not tested here, that
280 the reported zinc plasticity mechanism is a general mechanism that dynamically modulates
281 sensory processing for adaptation to different sensory environments and injury.
282

283 Whereas the exact synaptic, natural, and ethologically relevant stimuli that elicit zinc plasticity
284 remain unknown, here we developed an *in vitro* and *in vivo* model for studying bidirectional zinc
285 plasticity. This is a crucial step towards further elucidation of the detailed natural stimuli eliciting
286 zinc plasticity, as well as the precise cellular and molecular mechanisms underlying the induction
287 and expression of zinc plasticity. Moreover, our model will be useful for probing the behavioral
288 consequences of zinc plasticity and their underlying synaptic mechanisms, which remain
289 unknown.
290
291 **Mechanisms of Group 1 mGluR-mediated zinc plasticity**
292 Our results show that differential activation of Group 1 mGluRs, by either L/HFS or high/low
293 concentrations of DHPG, determines the induction and direction of zinc plasticity. Both LFS and
294 HFS induce mGluR-mediated glutamatergic plasticity in various central synapses. In the
295 hippocampus, LFS induces mGluR-LTD (Oliet et al., 1997; Huber et al., 2000), but when NMDARs
296 are blocked, mGluR-LTD is induced by HFS (Wu et al., 2001). In cerebellar climbing fibers, HFS
297 induces mGluR-LTD (Brasnjo & Otis, 2001; Dzubay & Otis, 2002), whereas in DCN PFs, mGluR
298 activation contributes to both HFS-induced LTP and LFS-induced LTD (Fujino & Oertel, 2003).
299 Our results show that prolonged LFS increases zinc signaling, similarly to Group 1 mGluR
300 activation with 50 μM DHPG; whereas, brief HFS reduces zinc signaling, similarly to activation
301 with 5 μM DHPG. This suggests that prolonged LFS activates Group 1 mGluR signaling differently
302 than brief HFS. Group 1 mGluRs, mGluR1 and mGluR5, are linked to the IP_3-Diacylglycerol (DAG)
303 signaling pathway, leading to intracellular rises in Ca^{2+} from intracellular stores (Abdul-Ghani et
304 al., 1996; Conn & Pin, 1997; Kim et al., 2008). We therefore propose, albeit not tested here, that
305 differential mGluR activation, by L/HFS, leads to subsequent release of different amounts or types
306 of intracellular Ca^{2+} signals. Different Ca^{2+} signals may in turn activate diverse signaling pathways
307 that ultimately lead to increased and decreased synaptic zinc levels. An analogue that comes to

mind is the mechanism via which differential activation of NMDARs, by various levels of synaptic activity, leads to variable Ca^{2+} levels and signaling, ultimately determining the induction of both LTP and LTD (Malenka & Bear, 2004).

In the DCN, cartwheel cells (CWCs) express Group 1 mGluRs, particularly mGluR1, suggesting that the locus of induction of zinc plasticity is postsynaptic (Wright et al., 1996). Because zinc plasticity involves modulation of presynaptic zinc levels, this would suggest the presence of a retrograde signal from CWCs involved in the expression of zinc plasticity in PFs. Alternatively, the presence of mGluR1 on axon terminals in the DCN molecular layer may support a presynaptic locus of induction (Bilak & Morest, 1998). Because ZnT3 determines vesicular zinc levels (Palmiter et al., 1996; Cole et al., 1999), modulation of ZnT3 expression or function may underlie the expression of zinc plasticity. In the retina, optic nerve injury increases ZnT3 immunostaining, supporting that increases in ZnT3 expression mediate increases in synaptic zinc levels (Li et al., 2017). Yet, in the barrel cortex after whisker plucking, ZnT3 protein and mRNA levels remain unchanged despite increases in vesicular zinc content (Liguz-Lecznar et al., 2005; Nakashima et al., 2011). As such, changes in barrel cortex synaptic zinc levels are more consistent with a modulation of ZnT3 function. In the context of ZnT3 modulation, it is interesting that the vesicular glutamate transporter 1 (VGlut1) is co-targeted to synaptic vesicles with ZnT3, and increases ZnT3 zinc transport (Salazar et al., 2005). Because VGlut1 is highly expressed in the DCN molecular layer (Zhou et al., 2007), one hypothesis is that modulation of VGlut1 may modulate ZnT3 function in PF terminals. However, noise-induced zinc plasticity does not affect presynaptic glutamate dynamics (Fig. 7 D), suggesting that zinc and glutamate signaling can be independently modulated. Therefore, a change in ZnT3 expression is a more likely candidate for mediating decreased synaptic zinc levels after noise exposure in the DCN. While our results reveal a role for Group 1 mGluRs and changes in presynaptic zinc levels for the induction and expression of

zinc plasticity, further support from additional experiments will be necessary to determine the detailed induction and expression mechanisms.

Implications of zinc plasticity for LTP and LTD

Low frequency stimulation typically induces glutamatergic LTD (Mulkey & Malenka, 1992; Fujino & Oertel, 2003), whereas HFS typically induces LTP (Malenka & Nicoll, 1993; Fujino & Oertel, 2003). Based on our findings, we propose that zinc plasticity by L/HFS may further enhance LTD and LTP. Namely, LFS increases zinc signaling, thereby increasing NMDA/AMPAR inhibition, which would further enhance the effects of glutamatergic LTD. HFS reduces zinc signaling, thereby reducing NMDA/AMPAR inhibition, which would further enhance LTP. Overall, zinc plasticity serves as a positive feedback mechanism to enhance the effects of LTP or LTD on glutamatergic synaptic transmission.

Zinc inhibits NMDARs and thus modulates the induction of NMDAR-dependent LTP and LTD in the hippocampus (Izumi et al., 2006; Takeda et al., 2009; Vergnano et al., 2014). As such, zinc plasticity may also contribute to 'metaplasticity', the modulation of subsequent LTP and LTD (Abraham & Tate, 1997). Based on our findings, HFS-dependent reductions in zinc signaling will promote subsequent NMDAR-dependent LTP and decrease subsequent NMDAR-dependent LTD. Conversely, increases in zinc signaling after LFS would inhibit subsequent NMDAR-LTP and enhance NMDAR-LTD. Together, zinc plasticity acts a positive feedback signal in NMDAR-dependent synaptic plasticity and metaplasticity.

In synapses expressing mGluR-dependent LTD (Oliet et al., 1997), zinc plasticity is also expected to act as a positive feedback signal, for LFS is expected to enhance zinc levels and further suppress glutamatergic transmission. However, in synapses expressing NMDAR-independent LTP, such as in hippocampal mossy fiber-CA3 synapses, zinc plasticity is not expected to act as

359 a positive feedback. Zinc contributes to mossy fiber presynaptic LTP in response to HFS (Pan et
360 al., 2011), and therefore if HFS reduces zinc levels in mossy fiber synapses, zinc plasticity will
361 act as negative feedback signal for subsequent LTP induction. Taken together, we propose that
362 the role of zinc plasticity in LTP and LTD depends on the specific mechanisms underlying LTP
363 and LTD, but zinc plasticity mostly acts as a positive feedback signal, especially for the most
364 abundant forms of LTP and LTD in the brain, which depend on NMDAR activation.
365
366 **Clinical and translational implications of zinc plasticity**
367 In the context of zinc plasticity as a positive feedback signal for NMDAR-dependent plasticity, it
368 is interesting that exposure to loud sound -- known to induce tinnitus -- decreases synaptic zinc
369 levels in the DCN. Such decreases could potentially lead to runaway excitation due to enhanced
370 LTP and decreased LTD, and thus to pathological DCN hyperactivity associated with tinnitus
371 (Tzounopoulos, 2008). Noise-induced pathological hyperexcitability through LTP/LTD-like
372 mechanisms in the DCN PF synapses has been hypothesized and recently implicated in tinnitus
373 treatment (Tzounopoulos, 2008; Marks et al., 2018), therefore suggesting that noise-induced
374 reductions in synaptic zinc might contribute to tinnitus.
375
376 In addition to a potential involvement of zinc signaling in tinnitus, pathological neuronal zinc
377 signaling is associated with numerous other neurological disorders, such as schizophrenia,
378 Alzheimer's disease, and autism. Variants in the ZnT3 gene are associated with schizophrenia
379 (Perez-Becerril et al., 2016); Alzheimer's patients display reduced levels of ZnT3 expression
380 (Olesen et al., 2016); ZnT3KO mice exhibit cognitive deficits similar to Alzheimer's and autism-
381 like phenotypes (Adlard et al., 2010; Yoo et al., 2016); and a zinc ionophore rescues behavioral
382 phenotypes in mouse models of autism (Lee et al., 2015). Therefore, there is converging evidence
383 that pathological zinc signaling may play a significant role in the cognitive deficits observed in
384 these neurological disorders. As such, understanding the cellular mechanisms that govern the

plasticity of zinc levels is a crucial first step in determining the molecular pathways that, when disrupted, may lead to pathological zinc levels. Furthermore, elucidating these mechanisms, such as the role of Group 1 mGluR signaling identified here, may lead to novel targets and approaches for treating pathological zinc signaling in disease states.

Materials and Methods

Animals

Male or female ICR mice (Envigo) were used in this study, aged between postnatal day 17 (P17) to P28. All animal procedures were approved by the Institutional Animal Care and Use Committee of the University of Pittsburgh, Pittsburgh, PA.

Brain slice preparation for electrophysiology and fluorescent imaging

Mice were deeply anesthetized with isoflurane (3% in O_2), then immediately decapitated and their brains were removed. Brain slices were prepared in artificial cerebrospinal fluid (ACSF, 34°C) containing the following (in mM): 130 NaCl, 3 KCl, 1.2 $CaCl_2 \cdot 2H_2O$, 1.3 $MgCl_2 \cdot 6H_2O$, 20 $NaHCO_3$, 3 HEPES, and 10 D-Glucose, saturated with 95% O_2/5% CO_2 (vol/vol), pH = 7.25-7.35, ~300 mOsm. Using a Vibratome (VT1200S; Leica), coronal brain slices (210 μm thickness) containing the left dorsal cochlear nucleus (DCN) were cut, then placed in a chamber containing warm (34°C) ACSF, and incubated for 60 min at 34°C, then room temperature (no longer than 3 hours) before beginning electrophysiology or imaging experiments. Incubating ACSF was the same as cutting ACSF, except it was stirred with Chelex 100 resin (Bio-Rad) for 1 hour to remove contaminating zinc, then filtered using Nalgene rapid flow filters lined with polyethersulfone (0.2 μm pore size). After filtering, high purity $CaCl_2 \cdot 2H_2O$ and $MgCl_2 \cdot 6H_2O$ (99.995%; Sigma Aldrich) were added. All plastic and glassware used for these experiments were washed with 5% nitric acid.

411 **Electrophysiology**

412 *Whole-cell recordings*. DCN slices were transferred to the recording chamber and perfused with
413 ACSF (1-2 mL/min), maintained at ~34°C using an inline heating system (Warner Instruments).
414 Recording ACSF was the same as incubating ACSF (see above), except it contained 2.4 mM
415 $CaCl_2{\cdot}2H_2O$. Whole-cell recordings from cartwheel cells were performed using glass micropipettes
416 (3-6 MΩ; Sutter Instruments). Cartwheel cells were identified by the presence of complex spikes
417 in cell-attached configuration before break-in or in response to current injections in current-clamp
418 mode after break-in (Zhang & Oertel, 1993; Manis et al., 1994; Tzounopoulos et al., 2004).
419 Recording pipettes were filled with a potassium-based internal solution (except for Fig. 6, see
420 below) containing the following (in mM): 113 K-gluconate, 4.5 $MgCl_2{\cdot}6H_2O$, 14 Tris-
421 phosphocreatine, 9 HEPES, 0.1 EGTA, 4 Na_2ATP, 0.3 Tris-GTP, and 10 sucrose (pH = 7.25, 295
422 mOsm). For experiments shown in Fig. 6 B-D measuring NMDAR EPSCs, recordings were
423 performed using a cesium-based internal solution containing the following (in mM): 128
424 $Cs(CH_3O_3S)$, 10 HEPES, 4 $MgCl_2{\cdot}6H_2O$, 4 Na_2ATP, 0.3 Tris-GTP, 10 Tris-phosphocreatine, 1
425 EGTA, 1 QX-314, and 3 Na-ascorbate (pH = 7.25, 300 mOsm). Recordings were performed using
426 ephus (Suter et al., 2010) and a MultiClamp 700B amplifier (Axon Instruments). Data were
427 sampled at 10 kHz and low-pass-filtered at 4 kHz. Series resistance (R_s) and input resistance
428 (R_m) were monitored during the recording period by delivering -5 mV voltage steps for 50 ms. R_s
429 was calculated by dividing the -5 mV voltage step by the peak current generated immediately
430 after the voltage step. R_m was calculated by dividing the -5 mV voltage step by the difference
431 between the baseline and steady-state hyperpolarized current, then subtracting R_s. Data were
432 excluded if R_s or R_m changed by more than 20% from the baseline period. EPSCs were evoked
433 using an Isoflex stimulator (A.M.P.I., 0.1 ms pulses) through a glass ACSF-containing theta
434 electrode to stimulate the zinc-rich parallel fibers. All EPSCs were recorded in the presence of
435 SR95531 (20 μM, $GABA_AR$ antagonist) and strychnine (1 μM, GlyR antagonist). AMPAR EPSCs
436 were recorded in voltage-clamp mode at -70 mV. For paired-pulse experiments, the inter-stimulus

interval was 50 ms. NMDAR EPSCs were evoked by a 5-pulse stimulus train (20 Hz) (Anderson et al., 2015), recorded in voltage clamp mode at +40 mV, and in the presence of DNQX (20 μM, AMPA/kainate receptor antagonist). All drugs were always bath applied.

Induction of plasticity. High-frequency stimulation (HFS) consisted of 3 trains of 100 Hz pulses for 1 sec, with 10 sec between trains. For the experiments shown in Fig. 1 C, a subset of cells (n=5) were depolarized to -10 mV during each HFS train, while the other subset (n=6) were held at -70 mV during HFS. Because we observed no difference in the zinc plasticity (EPSC % baseline after ZX1) between these subsets (depolarized = 102.7±5.4%, non-depolarized = 108.8±8.6%, p = 0.58, unpaired t test), they were grouped together for subsequent analysis. For all other experiments, cells were voltage-clamped at -70 mV during HFS. For experiments measuring NMDAR EPSCs after HFS (Fig. 6 B-D), DNQX (20 μM) was added after HFS, then cells were voltage-clamped at +40 mV to record NMDAR EPSCs. Low-frequency stimulation (LFS) consisted of 5 Hz pulses for 3 min. During LFS, cells were held at -80 mV in current-clamp mode. To isolate mGluR-mediated plasticity, all LFS experiments were performed in the presence of APV (50 μM, NMDAR antagonist), and with external ACSF containing 4 mM $CaCl_2{\cdot}2H_2O$ and 4 mM $MgCl_2{\cdot}6H_2O$ (Oliet et al., 1997). For normalized EPSCs (% baseline), EPSC amplitudes were normalized to the average EPSC amplitude during the 5 min baseline period before L/HFS, DHPG, or ZX1 application. To quantify ZX1 potentiation after L/HFS or DHPG application, EPSC amplitudes were renormalized to the average EPSC amplitude of the new baseline period 5 min before ZX1 application. ZX1 potentiation (shown in bar graphs) was quantified as the percent increase in the average EPSC amplitude during the last 5 min of ZX1 application compared to the 5 min baseline period before ZX1 application.

Vesicular zinc imaging with DA-ZP1

After preparation and incubation of DCN slices (described above), slices were transferred to the imaging chamber and perfused with recirculating ACSF (2-3 mL/min) maintained at ~34°C. Imaging of presynaptic vesicular zinc levels in DCN parallel fibers was performed using DA-ZP1, a high-affinity, membrane permeable fluorescent zinc sensor (Zastrow et al., 2016). DA-ZP1 (0.5 μM) was added to the ACSF, and allowed to incubate for at least 5-10 min before imaging. In order to quantify the effects of DHPG (Fig. 5) or noise exposure (Fig. 7A) compared to controls, pairs of treated and control slices were always imaged simultaneously in the same imaging chamber. Images were acquired using an upright microscope (Olympus BX5) with epifluorescence optics through a 20x water immersion objective. Green fluorescent signals were isolated using a Pinkel filter set (Semrock LF488/543/625-3X-A-000) in response to excitation by an ephus-driven blue LED (M470L2; Thorlabs), and images were acquired using a CCD camera (Retiga 2000R, QImaging). Images consisted of 20 frames captured at 0.2 Hz, which were then averaged together and analyzed using custom routines in MATLAB (Mathworks). In order to quantify zinc-sensitive fluorescence in the DCN molecular layer, a region of interest (ROI) within each slice was selected containing the zinc-rich molecular layer or the zinc-lacking deep layer (Zastrow et al., 2016; Kalappa et al., 2015). Fluorescence intensity was averaged within each ROI, and the zinc-sensitive fluorescence for each slice was calculated by subtracting the deep layer fluorescence from the molecular layer fluorescence. Zinc-sensitive fluorescence in treated slices (DHPG in Fig. 5B or noise exposure in Fig. 7A) was normalized to the simultaneously imaged control, non-treated, slice. For DHPG experiments (Fig. 5), DHPG (5 μM or 50 μM) was added to ACSF in the incubating chamber at least 20 min before initiating imaging. For experiments testing potential effects of ZX1 on DA-ZP1 fluorescence (Fig. 6E), imaging of ZX1-treated or control slices was performed in the presence or absence, respectively, of ZX1 (100 μM) in the external ACSF. For ZX1-treated slices, ZX1 was added to the ACSF 10 min before adding

DA-ZP1, then fluorescent images were acquired 10 min after DA-ZP1 application (20 min after ZX1 application).

Noise exposure

Noise exposure was performed based on previously published methods (Kalappa et al., 2015). Sham- or noise-exposed mice were anesthetized using 3% isoflurane during induction and 1-1.5% during maintenance. Noise-exposed mice were exposed for 4 hours to narrow bandpass noise at 116 dB sound pressure level (SPL), centered at 16 kHz with a 1.6 kHz bandwidth. Noise was presented unilaterally (left ear) through a pipette tip inserted into the left ear canal, with the other end attached to a calibrated speaker (CF-1; Tucker Davis Technologies). Sham-exposed mice underwent an identical procedure except without any noise exposure. For mice given intraperitoneal injections of AIDA (2 mg/kg) or vehicle (saline, 0.9% NaCl), one injection was given 30 min prior to exposure, and a second injection was given 2 hours later. After noise- or sham-exposure, ABRs were collected and mice recovered from anesthesia, then DCN slices were prepared (within 30 min after exposure).

ABRs

Auditory Brainstem Responses (ABRs) were measured based on previously published methods (Kalappa et al., 2015). ABRs were recorded immediately after noise- or sham-exposure. During ABR measurements, mice were anesthetized using 3% isoflurane during induction and 1-1.5% during maintenance. Mice were placed in a sound attenuating chamber and temperature was maintained at ~37°C using a heating pad. A subdermal electrode was placed at the vertex, the ground electrode placed ventral to the right pinna, and the reference electrode placed ventral to the left pinna (sham- or noise-exposed ear). For ABR measurements from contralateral ears of noise-exposed mice, the reference electrode was placed ventral to the right pinna (contralateral ear) and the ground electrode placed ventral to the left pinna. ABRs were detected in response

513 to 1 ms click sound stimuli, presented through a pipette tip inserted into the ear canal, with the
514 other end attached to the speaker (CF-1; Tucker Davis Technologies). ABRs were recorded in
515 response to clicks presented in 10 dB steps, ranging from 0-80 dB SPL. 1 ms clicks were
516 presented at a rate of 18.56/sec using System 3 software package from Tucker Davis
517 Technologies, and ABRs were averaged 512 times and filtered using a 300-3,000 Hz bandpass
518 filter. ABR threshold was defined as the lowest stimulus intensity which generated a reliable Wave
519 1 in the response waveform. Wave 1 amplitude was measured as the peak-to-trough amplitude
520 of the first wave in the ABR waveform (latency ~2 ms), in response to 80 dB SPL clicks.
521
522 **Drugs**
523 All chemicals used for ACSF and internal solutions were purchased from Sigma-Aldrich. The
524 following drugs were purchased from HelloBio: SR95531 hydrobromide, DL-AP5, DNQX
525 disodium salt, MPEP hydrochloride, LY367385, and (S)-3,5-Dihydroxyphenylglycine (DHPG).
526 Strychnine hydrochloride was purchased from Abcam. (S)-α-Methyl-4-carboxyphenylglycine
527 (MCPG) and (RS)-1-Aminoindan-1,5-dicarboxylic acid (AIDA) were purchased from Tocris. ZX1
528 was purchased from STREM Chemicals.
529
530 **Data analysis**
531 All data analysis was performed using Matlab (Mathworks), Excel (Microsoft), or Prism 7
532 (GraphPad). For statistical comparisons, we used one-sample *t* tests or unpaired *t* tests (between
533 groups) if the data passed the Shapiro-Wilk normality test. Welch's correction was used if
534 variances were significantly different (F test). For non-normally distributed data, we used Wilcoxon
535 signed rank tests or Mann-Whitney tests (between groups). Significance levels are defined as p
536 < 0.05. Group data are presented as mean ± SEM.
537
538

Acknowledgements

We thank Drs. Stephen Lippard and Jacob Goldberg from Massachusetts Institute of Technology for generously providing DA-ZP1.

Funding

National Institute on Deafness and Other Communication Disorders: R01-DC007905 (T.T.); F31-DC015924 (N.W.V.).

Author Contributions

N.W.V. performed experiments and analyzed data. N.W.V. and T.T. designed experiments and wrote the paper.

Ethics

All methods for animal handling, anesthesia, and sacrifice were approved by the Institutional Animal Care and Use Committee of the University of Pittsburgh, Pittsburgh, PA. The approved IACUC protocol numbers used for this study were: 14125118, 14094011, 17071036, and 17127808.

Competing Interests

The authors declare that no competing interests exist.

References

Abdul-Ghani MA, Valiante TA, Carlen PL, Pennefather PS. (1996). Metabotropic glutamate receptors coupled to IP3 production mediate inhibition of IAHP in rat dentate granule neurons. *J Neurophysiol*. Oct;76(4):2691-700. PMID: 8899638

565 Abraham WC, Tate WP. Metaplasticity: a new vista across the field of synaptic plasticity. *Prog*
566 *Neurobiol*. Jul;52(4):303-23. PMID: 9247968
567
568 Adlard PA, Parncutt JM, Finkelstein DI, Bush AI. (2010). Cognitive loss in zinc transporter-3
569 knock-out mice: a phenocopy for the synaptic and memory deficits of Alzheimer's disease? *J*
570 *Neurosci*. Feb 3;30(5):1631-6. PMID: 20130173
571
572 Anderson CT, Radford RJ, Zastrow ML, Zhang DY, Apfel UP, Lippard SJ, Tzounopoulos T.
573 (2015). *Proc Natl Acad Sci U S A*. May 19;112(20):E2705-14. PMID: 25947151
574
575 Anderson CT, Kumar M, Xiong S, Tzounopoulos T. (2017). Cell-specific gain modulation by
576 synaptically released zinc in cortical circuits of audition. *Elife*. Sep 9;6. pii: e29893. PMID:
577 28887876
578
579 Atallah BV, Bruns W, Carandini M, Scanziani M. (2012). Parvalbumin-expressing interneurons
580 linearly transform cortical responses to visual stimuli. *Neuron*. 2012 Jan 12;73(1):159-70.
581 PMID: 22243754
582
583 Auerbach BD, Rodrigues PV, Salvi RJ. (2014). Central gain control in tinnitus and hyperacusis.
584 *Front Neurol*. Oct 24;5:206. PMID: 25386157
585
586 Bilak SR, Morest DK. (1998). Differential expression of the metabotropic glutamate receptor
587 mGluR1alpha by neurons and axons in the cochlear nucleus: in situ hybridization and
588 immunohistochemistry. *Synapse*. Apr;28(4):251-70. PMID: 9517834
589

590 Brasnjo G, Otis TS. (2001). Neuronal glutamate transporters control activation of postsynaptic
591 metabotropic glutamate receptors and influence cerebellar long-term depression. *Neuron*.
592 Aug 30;31(4):607-16. PMID: 11545719
593
594 Brown CE, Dyck RH. (2002). Rapid, experience-dependent changes in levels of synaptic zinc in
595 primary somatosensory cortex of the adult mouse. *J Neurosci*. Apr 1;22(7):2617-25. PMID:
596 11923427
597
598 Brown CE, Dyck RH. (2005). Modulation of synaptic zinc in barrel cortex by whisker stimulation.
599 *Neuroscience*. 134(2):355-9. PMID: 16019150
600
601 Chambers AR, Resnik J, Yuan Y, Whitton JP, Edge AS, Liberman MC, Polley DB. (2016).
602 Central Gain Restores Auditory Processing following Near-Complete Cochlear Denervation.
603 *Neuron*. Feb 17;89(4):867-79. PMID: 26833137
604
605 Cole TB, Wenzel HJ, Kafer KE, Schwartzkroin PA, Palmiter RD. (1999). Elimination of zinc from
606 synaptic vesicles in the intact mouse brain by disruption of the ZnT3 gene. *Proc Natl Acad*
607 *Sci U S A*. Feb 16;96(4):1716-21. PMID: 9990090
608
609 Conn PJ, Pin JP. (1997). Pharmacology and functions of metabotropic glutamate receptors.
610 *Annu Rev Pharmacol Toxicol*. 37:205-37. PMID: 9131252
611
612 Danscher G, Stoltenberg M. (2005). Zinc-specific autometallographic in vivo selenium methods:
613 tracing of zinc-enriched (ZEN) terminals, ZEN pathways, and pools of zinc ions in a
614 multitude of other ZEN cells. *J Histochem Cytochem*. Feb;53(2):141-53. PMID: 15684327
615

Dean I, Harper NS, McAlpine D. (2005). Neural population coding of sound level adapts to stimulus statistics. *Nat Neurosci*. Dec;8(12):1684-9. PMID: 16286934

Dyck RH, Chaudhuri A, Cynader MS. (2003). Experience-dependent regulation of the zincergic innervation of visual cortex in adult monkeys. *Cereb Cortex*. Oct;13(10):1094-109. PMID: 12967926

Dzubay JA, Otis TS. Climbing fiber activation of metabotropic glutamate receptors on cerebellar purkinje neurons. *Neuron*. Dec 19;36(6):1159-67. PMID: 12495629

Frederickson CJ, Howell GA, Haigh MD, Danscher G. (1988). Zinc-containing fiber systems in the cochlear nuclei of the rat and mouse. *Hear Res*. Nov;36(2-3):203-11. PMID: 3209493

Frederickson CJ, Koh JY, Bush AI. (2005). The neurobiology of zinc in health and disease. *Nat Rev Neurosci*. Jun;6(6):449-62. PMID: 15891778

Fujino K, Oertel D. (2003). Bidirectional synaptic plasticity in the cerebellum-like mammalian dorsal cochlear nucleus. *Proc Natl Acad Sci U S A*. Jan 7;100(1):265-70. PMID: 12486245

Huber KM, Kayser MS, Bear MF. (2000). Role for rapid dendritic protein synthesis in hippocampal mGluR-dependent long-term depression. *Science*. May 19;288(5469):1254-7. PMID: 10818003

Huber KM, Roder JC, Bear MF. (2001). Chemical induction of mGluR5- and protein synthesis--dependent long-term depression in hippocampal area CA1. J Neurophysiol. Jul;86(1):321-5. PMID: 11431513

642 Izumi Y, Auberson YP, Zorumski CF. (2006). Zinc modulates bidirectional hippocampal plasticity
643 by effects on NMDA receptors. *J Neurosci*. Jul 5;26(27):7181-8. PMID: 16822975
644
645 Kalappa BI, Anderson CT, Goldberg JM, Lippard SJ, Tzounopoulos T. (2015). AMPA receptor
646 inhibition by synaptically released zinc. *Proc Natl Acad Sci U S A*. Dec 22;112(51):15749-
647 54. PMID: 26647187
648
649 Kalappa BI, Tzounopoulos T. (2017). Context-Dependent Modulation of Excitatory Synaptic
650 Strength by Synaptically Released Zinc. *eNeuro*. 2017 Mar 3;4(1). PMID: 28275718
651
652 Kim CH, Lee J, Lee JY, Roche KW. (2008). Metabotropic glutamate receptors: phosphorylation
653 and receptor signaling. *J Neurosci Res*. Jan;86(1):1-10. PMID: 17663464
654
655 Kujawa SG, Liberman MC. (2009). Adding insult to injury: cochlear nerve degeneration after
656 "temporary" noise-induced hearing loss. *J Neurosci*. Nov 11;29(45):14077-85. PMID:
657 19906956
658
659 Lee EJ, Lee H, Huang TN, Chung C, Shin W, Kim K, Koh JY, Hsueh YP, Kim E. (2015). Trans-
660 synaptic zinc mobilization improves social interaction in two mouse models of autism
661 through NMDAR activation. *Nat Commun*. May 18;6:7168. PMID: 25981743
662
663 Li Y, Andereggen L, Yuki K, Omura K, Yin Y, Gilbert HY, Erdogan B, Asdourian MS, Shrock C,
664 de Lima S, Apfel UP, Zhuo Y, Hershfinkel M, Lippard SJ, Rosenberg PA, Benowitz L.
665 (2017). Mobile zinc increases rapidly in the retina after optic nerve injury and regulates
666 ganglion cell survival and optic nerve regeneration. *Proc Natl Acad Sci U S A*. Jan
667 10;114(2):E209-E218. PMID: 28049831

668 Liguz-Lecznar M, Nowicka D, Czupryn A, Skangiel-Kramska J. (2005). Dissociation of synaptic
669 zinc level and zinc transporter 3 expression during postnatal development and after sensory
670 deprivation in the barrel cortex of mice. *Brain Res Bull*. Jul 30;66(2):106-13. PMID:
671 15982526
672
673 Malenka RC, Nicoll RA. (1993). NMDA-receptor-dependent synaptic plasticity: multiple forms
674 and mechanisms. *Trends Neurosci*. Dec;16(12):521-7. PMID: 7509523
675
676 Malenka RC, Bear MF. (2004). LTP and LTD: an embarrassment of riches. *Neuron*. Sep
677 30;44(1):5-21. PMID: 15450156
678
679 Manis PB, Spirou GA, Wright DD, Paydar S, Ryugo DK. (1994). Physiology and morphology of
680 complex spiking neurons in the guinea pig dorsal cochlear nucleus. *J Comp Neurol*. Oct
681 8;348(2):261-76. PMID: 7814691
682
683 Marks KL, Martel DT, Wu C, Basura GJ, Roberts LE, Schvartz-Leyzac KC, Shore SE. (2018).
684 Auditory-somatosensory bimodal stimulation desynchronizes brain circuitry to reduce
685 tinnitus in guinea pigs and humans. *Sci Transl Med*. Jan 3;10(422). PMID: 29298868
686
687 McAllister BB, Dyck RH. (2017). Zinc transporter 3 (ZnT3) and vesicular zinc in central nervous
688 system function. *Neurosci Biobehav Rev*. Sep;80:329-350. PMID: 28624432
689
690 Mulkey RM, Malenka RC. (1992). Mechanisms underlying induction of homosynaptic long-term
691 depression in area CA1 of the hippocampus. *Neuron*. Nov;9(5):967-75. PMID: 1419003
692

693 Nakashima AS, Dyck RH. (2009). Zinc and cortical plasticity. *Brain Res Rev*. Mar;59(2):347-73.
694 PMID: 19026685
695
696 Nakashima AS, Butt RH, Dyck RH. (2011). Alterations in protein and gene expression within the
697 barrel cortices of ZnT3 knockout mice: experience-independent and dependent changes.
698 *Neurochem Int*. Nov;59(6):860-70. PMID: 21871936
699
700 Natan RG, Carruthers IM, Mwilambwe-Tshilobo L, Geffen MN. (2017). Gain Control in the
701 Auditory Cortex Evoked by Changing Temporal Correlation of Sounds. *Cereb Cortex*. Mar
702 1;27(3):2385-2402. PMID: 27095823
703
704 Ohshiro T, Angelaki DE, DeAngelis GC. (2011). A normalization model of multisensory
705 integration. *Nat Neurosci*. Jun;14(6):775-82. PMID: 21552274
706
707 Olesen RH, Hyde TM, Kleinman JE, Smidt K, Rungby J, Larsen A. (2016). Obesity and age-
708 related alterations in the gene expression of zinc-transporter proteins in the human brain.
709 *Transl Psychiatry*. Jun 14;6(6):e838. PMID: 27300264
710
711 Oliet SH, Malenka RC, Nicoll RA. (1997). Two distinct forms of long-term depression coexist in
712 CA1 hippocampal pyramidal cells. *Neuron*. Jun;18(6):969-82. PMID: 9208864
713
714 Palmiter RD, Cole TB, Quaife CJ, Findley SD. (1996). ZnT-3, a putative transporter of zinc into
715 synaptic vesicles. *Proc Natl Acad Sci U S A*. Dec 10;93(25):14934-9. PMID: 8962159
716

717 Pan E, Zhang XA, Huang Z, Krezel A, Zhao M, Tinberg CE, Lippard SJ, McNamara JO. (2011).
718 Vesicular zinc promotes presynaptic and inhibits postsynaptic long-term potentiation of
719 mossy fiber-CA3 synapse. *Neuron*. Sep 22;71(6):1116-26. PMID: 21943607
720
721 Paoletti P, Ascher P, Neyton J. (1997). High-affinity zinc inhibition of NMDA NR1-NR2A
722 receptors. *J Neurosci*. Aug 1;17(15):5711-25. PMID: 9221770
723
724 Perez-Becerril C, Morris AG, Mortimer A, McKenna PJ, de Belleroche J. (2016). Common
725 variants in the chromosome 2p23 region containing the SLC30A3 (ZnT3) gene are
726 associated with schizophrenia in female but not male individuals in a large collection of
727 European samples. *Psychiatry Res*. Dec 30;246:335-340. PMID: 27750116
728
729 Perez-Rosello T, Anderson CT, Schopfer FJ, Zhao Y, Gilad D, Salvatore SR, Freeman BA,
730 Hershfinkel M, Aizenman E, Tzounopoulos T. (2013). Synaptic Zn2+ inhibits
731 neurotransmitter release by promoting endocannabinoid synthesis. *J Neurosci*. May
732 29;33(22):9259-72. PMID: 23719795
733
734 Rabinowitz NC, Willmore BD, Schnupp JW, King AJ. (2011). Contrast gain control in auditory
735 cortex. *Neuron*. Jun 23;70(6):1178-91. PMID: 21689603
736
737 Resnik J, Polley DB. (2017). Fast-spiking GABA circuit dynamics in the auditory cortex predict
738 recovery of sensory processing following peripheral nerve damage. *Elife*. Mar 21;6. pii:
739 e21452. PMID: 28323619
740

741 Rubio ME, Juiz JM. (1998). Chemical anatomy of excitatory endings in the dorsal cochlear
742 nucleus of the rat: differential synaptic distribution of aspartate aminotransferase, glutamate,
743 and vesicular zinc. *J Comp Neurol*. Sep 28;399(3):341-58. PMID: 9733082
744
745 Salazar G, Craige B, Love R, Kalman D, Faundez V. (2005). Vglut1 and ZnT3 co-targeting
746 mechanisms regulate vesicular zinc stores in PC12 cells. J Cell Sci. May 1;118(Pt 9):1911-
747 21. PMID: 15860731
748
749 Snyder EM, Philpot BD, Huber KM, Dong X, Fallon JR, Bear MF. (2001). Internalization of
750 ionotropic glutamate receptors in response to mGluR activation. *Nat Neurosci*.
751 Nov;4(11):1079-85. PMID: 11687813
752
753 Suter BA, O'Connor T, Iyer V, Petreanu LT, Hooks BM, Kiritani T, Svoboda K, Shepherd GM.
754 (2010). Ephus: multipurpose data acquisition software for neuroscience experiments. *Front*
755 *Neural Circuits*. Aug 26;4:100. PMID: 21960959
756
757 Takeda A, Fuke S, Ando M, Oku N. (2009). Positive modulation of long-term potentiation at
758 hippocampal CA1 synapses by low micromolar concentrations of zinc. *Neuroscience*. Jan
759 23;158(2):585-91. PMID: 18984033
760
761 Tzounopoulos T. (2008). Mechanisms of synaptic plasticity in the dorsal cochlear nucleus:
762 plasticity-induced changes that could underlie tinnitus. *Am J Audiol*. Dec;17(2):S170-5.
763 PMID: 18978197
764
765 Tzounopoulos T, Kim Y, Oertel D, Trussell LO. (2004). Cell-specific, spike timing-dependent
766 plasticities in the dorsal cochlear nucleus. *Nat Neurosci*. Jul;7(7):719-25. PMID: 15208632

767 Tzounopoulos T, Rubio ME, Keen JE, Trussell LO. (2007). Coactivation of pre- and
768 postsynaptic signaling mechanisms determines cell-specific spike-timing-dependent
769 plasticity. *Neuron*. Apr 19;54(2):291-301. PMID: 17442249
770
771 Vergnano AM, Rebola N, Savtchenko LP, Pinheiro PS, Casado M, Kieffer BL, Rusakov DA,
772 Mulle C, Paoletti P. (2014). Zinc dynamics and action at excitatory synapses. *Neuron*. Jun
773 4;82(5):1101-14. PMID: 24908489
774
775 Vogt K, Mellor J, Tong G, Nicoll R. (2000). The actions of synaptically released zinc at
776 hippocampal mossy fiber synapses. *Neuron*. 2000 Apr;26(1):187-96. PMID: 10798403
777
778 Watkins PV, Barbour DL. (2008). Specialized neuronal adaptation for preserving input
779 sensitivity. *Nat Neurosci*. Nov;11(11):1259-61. PMID: 18820690
780
781 Wiśniewski K, Car H. (2002). (S)-3,5-DHPG: a review. CNS Drug Rev. Spring;8(1):101-16.
782 PMID: 12070529
783
784 Wright DD, Blackstone CD, Huganir RL, Ryugo DK. (1996). Immunocytochemical localization of
785 the mGluR1 alpha metabotropic glutamate receptor in the dorsal cochlear nucleus. *J Comp*
786 *Neurol*. Jan 22;364(4):729-45. PMID: 8821458
787
788 Wu J, Rush A, Rowan MJ, Anwyl R. (2001). NMDA receptor- and metabotropic glutamate
789 receptor-dependent synaptic plasticity induced by high frequency stimulation in the rat
790 dentate gyrus in vitro. *J Physiol.* Jun 15;533(Pt 3):745-55. PMID: 11410631
791

792 Yoo MH, Kim TY, Yoon YH, Koh JY. (2016). Autism phenotypes in ZnT3 null mice: Involvement
793 of zinc dyshomeostasis, MMP-9 activation and BDNF upregulation. *Sci Rep*. Jun
794 29;6:28548. PMID: 27352957
795
796 Zastrow ML, Radford RJ, Chyan W, Anderson CT, Zhang DY, Loas A, Tzounopoulos T, Lippard
797 SJ. (2016). Reaction-Based Probes for Imaging Mobile Zinc in Live Cells and Tissues. *ACS*
798 *Sens*. 2016 Jan 22;1(1):32-39. PMID: 26878065
799
800 Zhang S, Oertel D. (1993). Cartwheel and superficial stellate cells of the dorsal cochlear
801 nucleus of mice: intracellular recordings in slices. *J Neurophysiol*. May;69(5):1384-97. PMID:
802 8389821
803
804 Zhao Y, Tzounopoulos T. (2011). Physiological activation of cholinergic inputs controls
805 associative synaptic plasticity via modulation of endocannabinoid signaling. *J Neurosci*. Mar
806 2;31(9):3158-68. PMID: 21368027
807
808 Zhou J, Nannapaneni N, Shore S. (2007). Vessicular glutamate transporters 1 and 2 are
809 differentially associated with auditory nerve and spinal trigeminal inputs to the cochlear
810 nucleus. *J Comp Neurol*. Feb 1;500(4):777-87. PMID: 17154258
811
812
813 **Figure Legends**
814 **Figure 1. High-frequency stimulation (HFS) reduces synaptic zinc signaling in DCN parallel**
815 **fibers. (A)** Schematic of experimental setup illustrating stimulation of zinc-rich glutamatergic DCN
816 parallel fibers (PFs) and whole-cell recording of a postsynaptic cartwheel cell (CWC). **(B)** *Left:*
817 Time course of AMPAR EPSC amplitude before and after ZX1 application, normalized to baseline

before ZX1 application (100 μM). *Right:* Example AMPAR EPSCs before and after ZX1 application, showing ZX1 potentiation **(C)** *Left:* Time course of AMPAR EPSC amplitude before and after HFS, and before and after subsequent ZX1 application (blue). After obtaining a stable baseline, HFS was delivered (3 x 100 Hz for 1 sec, 10 sec ISI). To examine ZX1 potentiation after HFS, after obtaining a stable baseline after HFS, AMPAR EPSC amplitude was renormalized to the new baseline before ZX1 application. The renormalization is indicated by a gap and restart of timing in the x-axis. For comparison, red line shows normalized time course of AMPAR EPSC amplitude before and after ZX1 application in controls replotted from **B**. *Right:* Example AMPAR EPSCs showing no ZX1 potentiation after HFS. **(D)** Average ZX1 potentiation (% increase from baseline) during the last 5 min of ZX1 application. 'Control': 34.47 ± 5.7%, n=10, *p=0.0002, one-sample t test vs. 0%. 'HFS': 6.0 ± 5.15%, n=11, n.s. p=0.27, one-sample t test vs. 0%. 'Control' vs. 'HFS': *p=0.002, unpaired t test. The change in ZX1 potentiation is termed zinc plasticity. Values represent mean ± SEM. Star (*) indicates p<0.05.

Figure 2. Group 1 mGluR activation is required for HFS-induced zinc plasticity. (A) Time course of AMPAR EPSC amplitude before and after HFS in the presence of APV (50 μM), and before and after subsequent ZX1 application. **(B)** Same time course as in **A** but in the presence of LY367385 (100 μM), MPEP (4 μM), and APV (50 μM). For **(A-B)**, to examine ZX1 potentiation after HFS, similar approach and renormalization as in **1C** was performed. Red line shows the time course of AMPAR EPSC amplitude before and after ZX1 application in controls replotted from **1B**. Example traces show AMPAR EPSCs before and after ZX1. **(C)** Average ZX1 potentiation (% increase from baseline) during the last 5 min of ZX1 application, shown with control data from **1B**. 'HFS + APV': 4.28 ± 6.08%, n=9, n.s. p=0.502, one-sample t test vs. 0%. 'HFS + LY367385, MPEP, APV': 36.07 ± 9.05%, n=5, *p=0.016, one-sample t test vs. 0%. 'Control' vs. 'HFS + APV':

842 *p=0.002, unpaired t test. 'HFS + APV' vs. 'HFS + LY367385, MPEP, APV': *p=0.011, unpaired t
843 test. Values represent mean ± SEM. Star (*) indicates p<0.05.
844
845 **Figure 3. Low frequency stimulation (LFS) increases synaptic zinc signaling in DCN PFs,**
846 **and requires Group 1 mGluRs. (A)** Time course of AMPAR EPSC amplitude before and after
847 LFS (5 Hz, 3 min), and before and after subsequent ZX1 application (cyan); and similar time
848 course in interleaved control experiments (without LFS, red). **(B)** Same time course as in **A** but in
849 the presence of LY367385 (100 μM) and MPEP (4 μM) (green). Red line shows similar time
850 course in controls replotted from **A**. For **(A-B)**, to isolate mGluR-dependent plasticity, all
851 experiments were performed in the presence of APV (50 μM), and with ACSF containing 4 mM
852 Ca^{2+} and 4 mM Mg^{2+}. To examine ZX1 potentiation after LFS, similar approach and
853 renormalization as in **1C** was performed. Example traces show AMPAR EPSCs before and after
854 ZX1. **(C)** Average ZX1 potentiation (% increase from baseline) during the last 5 min of ZX1
855 application. 'Control': 19.65 ± 4.3%, n=5, *p=0.01, one-sample t test vs. 0%. 'LFS': 57.86 ± 12.4%,
856 n=6, *p=0.005, one-sample t test vs. 0%. 'LFS + LY367385, MPEP': 22.18 ± 8.3%, n=6, *p=0.04,
857 one-sample t test vs. 0%. 'Control' vs. 'LFS': *p=0.026, unpaired t test with Welch's correction.
858 'LFS' vs. 'LFS + LY367385, MPEP': *p=0.038, unpaired t test. Values represent mean ± SEM.
859 Star (*) indicates p<0.05.
860
861 **Figure 4. Group 1 mGluR activation is sufficient to induce bidirectional zinc plasticity. (A)**
862 Time course of AMPAR EPSC amplitude before and after application of 50 μM DHPG, and before
863 and after subsequent ZX1 application. **(B)** Time course of AMPAR EPSC amplitude before and
864 after application of 5 μM DHPG, and before and after subsequent ZX1 application. For **(A-B)**,
865 after obtaining a stable baseline, DHPG was applied. To examine ZX1 potentiation after DHPG
866 application, after obtaining a stable baseline after DHPG, AMPAR EPSC amplitude was

867 renormalized to the new baseline before ZX1 application. The renormalization is indicated by a
868 gap and restart of timing in the x-axis. **(C)** Time course of AMPAR EPSC amplitude before and
869 after ZX1 application after 50 μM DHPG (cyan), after 5 μM DHPG (purple), and in control (red
870 line, replotted from **1B**). Example traces show AMPAR EPSCs before and after ZX1. **(D)** Average
871 ZX1 potentiation (% increase from baseline) during the last 5 min of ZX1 application, shown with
872 control data from **1B**. 'DHPG (50 μM)': 93.51 ± 10.92%, n=5, *p= 0.001, one-sample t test vs. 0%.
873 'DHPG (5 μM)': 0.44 ± 7.08%, n=5, n.s. p=0.95, one-sample t test vs. 0%. 'Control' vs. 'DHPG (50
874 μM)': *p=0.0001, unpaired t test. 'Control' vs. 'DHPG (5 μM)': *p=0.003, unpaired t test. Values
875 represent mean ± SEM. Star (*) indicates p<0.05.
876
877 **Figure 5. Group 1 mGluR activation bidirectionally modulates presynaptic zinc levels in**
878 **DCN PFs. (A)** *Left:* Schematic of DA-ZP1 imaging of presynaptic zinc levels, illustrating the
879 molecular and deep layers of the DCN in brain slices. *Right:* Example of DA-ZP1 presynaptic
880 zinc-mediated fluorescent signals in the molecular layer, in control, after 50 μM DHPG, and after
881 5 μM DHPG. **(B)** Average DA-ZP1 (0.5 μM) fluorescence in DCN slices incubated with 50 μM or
882 5 μM DHPG, normalized to simultaneously imaged control slices. 'DHPG (50 μM)': 153.9 ±
883 13.42%, n=6, *p=0.01, one-sample t test vs. 100%. 'DHPG (5 μM)': 79.68 ± 6.66%, n=6, *p=0.028,
884 one-sample t test vs. 100%. Values represent mean ± SEM. Star (*) indicates p<0.05.
885
886 **Figure 6. Zinc plasticity does not depend on AMPAR plasticity, and it affects zinc-mediated**
887 **inhibition of NMDARs. (A)** Plot of AMPAR EPSC amplitude after ZX1 (% baseline before ZX1)
888 versus AMPAR EPSC amplitude changes after HFS (% baseline before HFS) for the experiments
889 included in Figs. **1C** and **2A-B**, showing no correlation between AMPAR plasticity and subsequent
890 potentiation by ZX1. Pearson r=0.1, n.s. p=0.63. Red line shows linear regression fit. **(B)** *Left:*
891 Time course of AMPAR EPSC amplitude before and after HFS, and NMDAR EPSC amplitude

892 before and after subsequent ZX1 application (blue); and similar time course in interleaved control
893 experiments (without HFS, red). *Right*: Example NMDAR EPSCs before and after ZX1
894 application. **(C)** Same time course as in **B** but in the presence of LY367385 (100 μM) and MPEP
895 (4 μM) (green). Red line shows similar time course in controls replotted from **B**. Example traces
896 show NMDAR EPSCs before and after ZX1. For **(B-C)**, after obtaining a stable baseline of
897 AMPAR EPSCs, HFS was delivered, then DNQX (20 μM) was applied. NMDAR EPSCs were
898 then recorded at +40 mV normalized to the baseline NMDAR EPSC amplitude before ZX1
899 application. The switch from AMPAR to NMDAR EPSC timecourse, and the renormalization of
900 EPSC amplitude are indicated by a gap and restart of timing in the x-axis. **(D)** Average ZX1
901 potentiation (% increase from baseline) during the last 5 min of ZX1 application. 'Control': 37.1 ±
902 3.1%, n=5, *p=0.0003, one-sample t test vs. 0%. 'HFS': 9.2 ± 5.2%, n=6, n.s. p=0.16, Wilcoxon
903 signed rank test vs. 0%. 'HFS + LY267385, MPEP': 42.6 ± 8.2%, n=5, *p=0.007, one-sample t
904 test vs. 0%. 'Control' vs 'HFS': *p=0.009, Mann Whitney test. 'HFS' vs 'HFS + LY367385, MPEP':
905 *p=0.03, Mann Whitney test. **(E)** *Left:* Example of DA-ZP1 presynaptic zinc-mediated fluorescent
906 signals in the DCN molecular layer, in control and ZX1-treated slices. For ZX1-treated slices, ZX1
907 (100 μM) was applied 10 min before DA-ZP1 and maintained throughout the experiments. *Right:*
908 Average DA-ZP1 (0.5 μM) fluorescence (arbitrary units) in control and ZX1-treated slices.
909 'Control': 27.16 ± 5.92, n=5. 'ZX1': 24.76 ± 5.78, n=5. 'Control' vs. 'ZX1': n.s. p=0.78, unpaired t
910 test. For **(D-E)**, values represent mean ± SEM. Star (*) indicates p<0.05.
911
912 **Figure 7. Sound-dependent zinc plasticity requires Group 1 mGluRs. (A)** *Left:* Example of
913 DA-ZP1 presynaptic zinc-mediated fluorescent signals in the DCN molecular layer, in slices from
914 sham-exposed mice (Control), noise-exposed mice (N.E.), N.E. AIDA-treated mice (N.E. + AIDA),
915 N.E. vehicle-treated mice (N.E. + veh.), and sham-exposed AIDA-treated mice (sham + AIDA).
916 *Right:* Average DA-ZP1 (0.5 μM) fluorescence for the same groups as on the *left*, normalized to

simultaneously imaged control slices from sham-exposed mice. 'N.E.': 41.12 ± 17.38%, n=6, *p=0.019, one-sample t test vs. 100%. 'N.E. + AIDA': 126.3 ± 30.67%, n=6, n.s. p=0.844, Wilcoxon signed rank test vs. 100%. 'N.E. + veh.': 47.75 ± 16.16%, n=5, *p=0.032, one-sample t test vs. 100%. 'Sham + AIDA': 96.33 ± 16.77%, n=6, n.s. p=0.836, one-sample t test vs. 100%. **(B)** Time course of AMPAR EPSC amplitude before and after ZX1 application in slices from N.E. mice (gray) and N.E. AIDA-treated mice (orange). Example traces show AMPAR EPSCs before and after ZX1. **(C)** Average ZX1 potentiation (% increase from baseline) during the last 5 min of ZX1 application. 'N.E.': 11.7 ± 8.56%, n=5, n.s. p=0.24, one-sample t test vs. 0%. 'N.E. + AIDA': 43.8 ± 8.05%, n=6, *p=0.003, one-sample t test vs. 0%. 'N.E.' vs 'N.E. + AIDA': *p=0.024, unpaired t test. **(D)** *Left:* Average paired-pulse ratio (PPR, pulse 2 / pulse 1) of baseline AMPAR EPSCs in slices from N.E. mice and N.E. AIDA-treated mice. 'N.E.': 1.896 ± 0.19, n=5. 'N.E. + AIDA: 2.056 ± 0.12, n=6. 'N.E.' vs 'N.E. + AIDA': n.s. p=0.476, unpaired t test. Example traces show AMPAR EPSCs in response to two pulses. *Right:* coefficient of variation (CV) analysis ($1/CV^2$) of baseline AMPAR EPSCs (pulse 1) in slices from N.E. mice and N.E. AIDA-treated mice, normalized to N.E. mice. 'N.E. + AIDA: 0.78 ± 0.22, n=6; n.s. p=0.44, Wilcoxon signed rank test vs. 1. **(E)** Example Auditory Brainstem Responses (ABRs, 10-80 dB SPL sound stimuli) from sham-exposed mice (recorded from sham-exposed, ipsilateral ear, black), N.E. mice (gray), and N.E. AIDA-treated mice (orange). Because no ABRs were detected in the ipsilateral ears of N.E. mice, ABRs were measured from ears contralateral to noise exposure. **(F)** *Left:* Average ABR thresholds (dB SPL): 'Sham ipsi.': 43.75 ± 3.24, n=8. 'N.E. contra.': 68 ± 3.74, n=5. 'N.E. + AIDA contra.': 65.71 ± 2.97, n=7. 'Sham ipsi.' vs 'N.E. contra.': *p=0.0006, unpaired t test. 'Sham ipsi. vs "N.E. + AIDA contra.': *p=0.002, Mann Whitney test. *Right:* Average ABR Wave I amplitude (μV): 'Sham ipsi.': 2.67 ± 0.31, n=8. 'N.E. contra.': 1.28 ± 0.15, n=5. 'N.E. + AIDA contra.': 1.25 ± 0.27, n=7. 'Sham ipsi.' vs 'N.E. contra.': *p=0.006, unpaired t test. 'Sham ipsi.' vs 'N.E. + AIDA

941 contra.': *p=0.006, Mann Whitney test. For **(A, C-D, F)**, values represent mean ± SEM. Star (*)

942 indicates p<0.05.

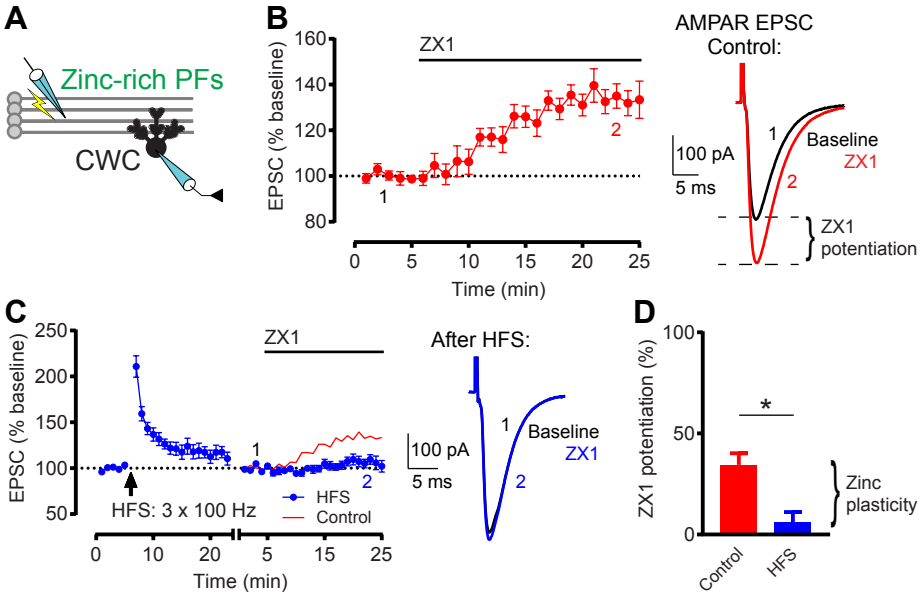

Figure 1

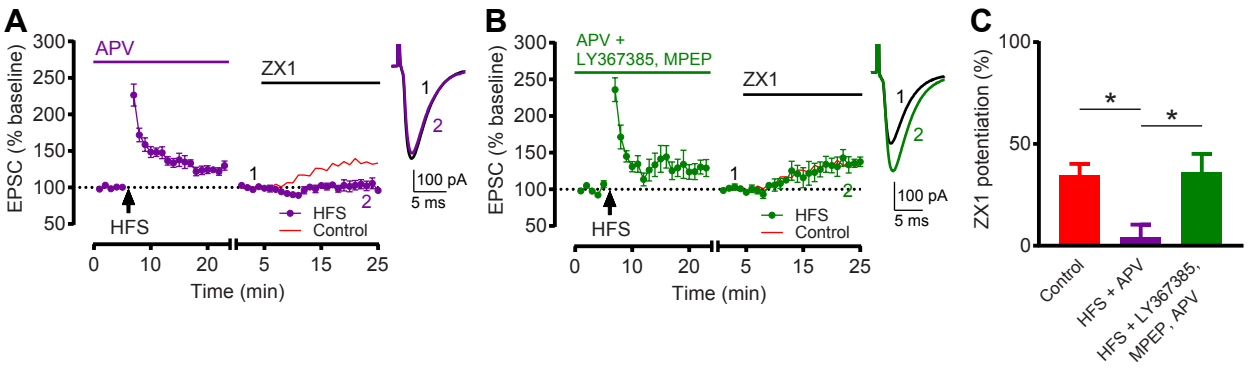

Figure 2

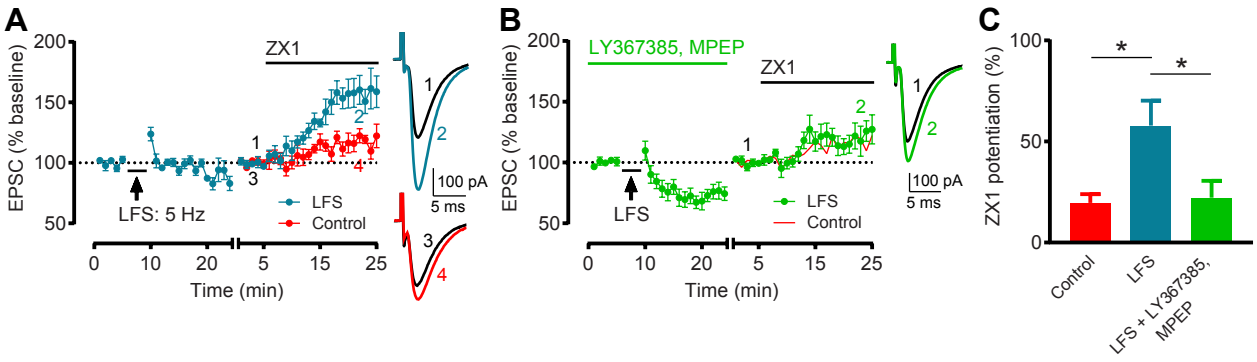

Figure 3

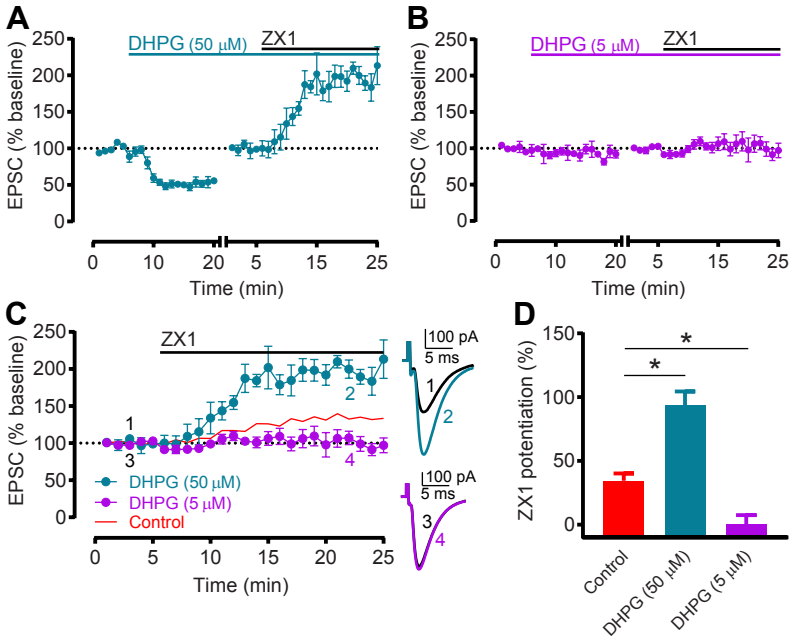

Figure 4

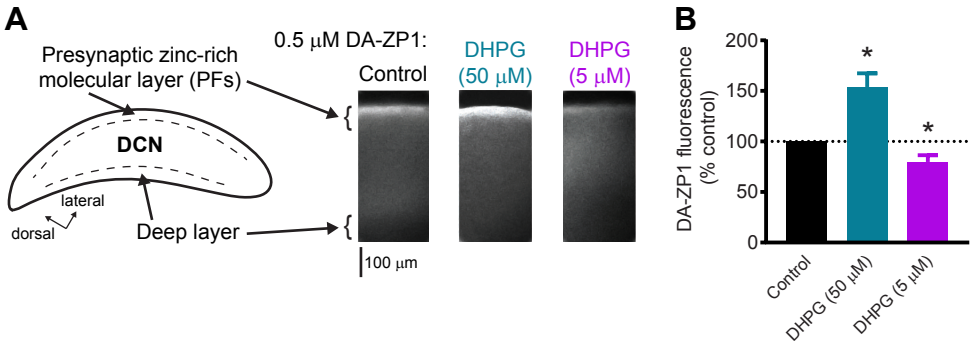

Figure 5

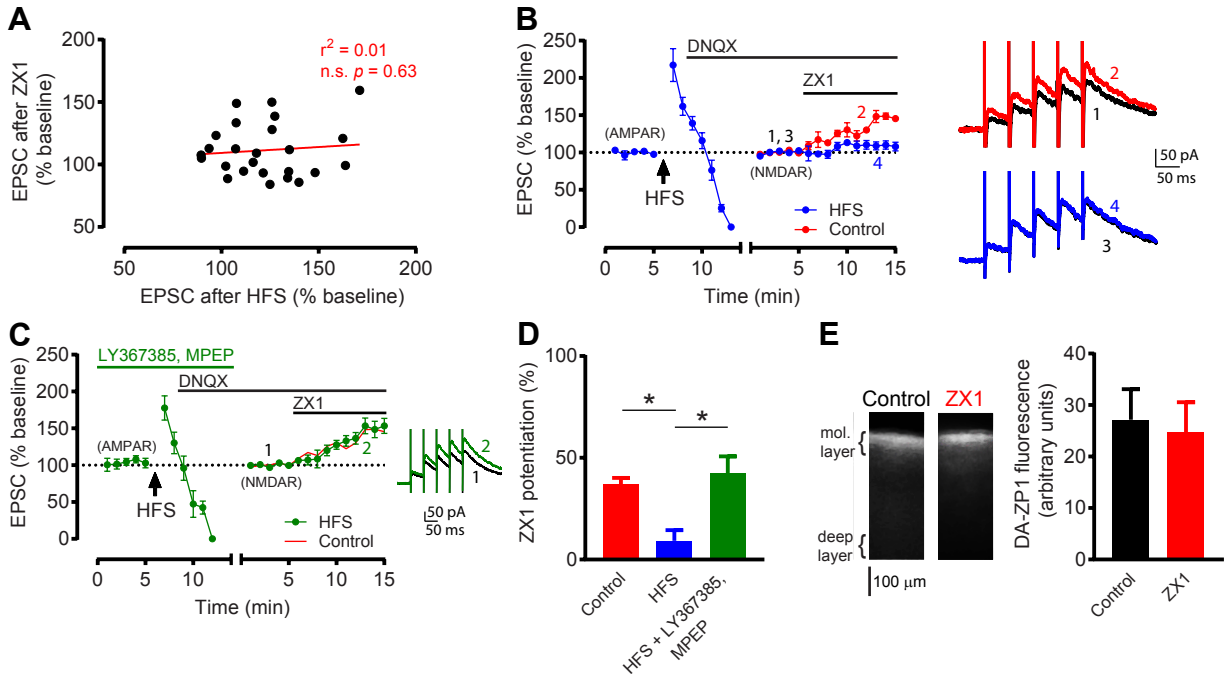

Figure 6

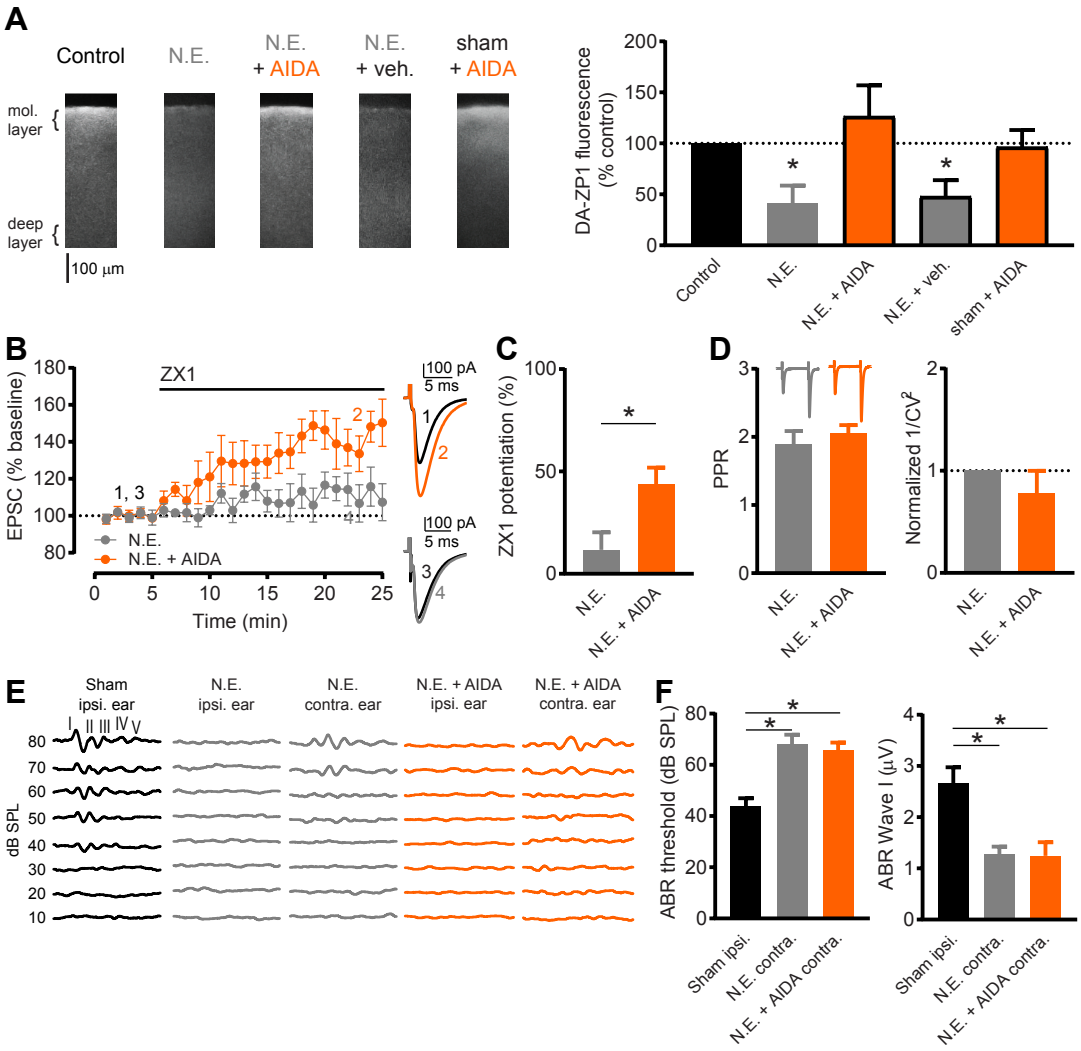

Figure 7